Quantum chaos in small quantum networks

Ilki Kim and Günter Mahler
Institut für Theoretische Physik I, Universität Stuttgart
Pfaffenwaldring 57, 70550 Stuttgart, Germany
phone: ++49-(0)711 685-5100, FAX: ++49-(0)711 685-4909
email: ikim@theo.physik.uni-stuttgart.de

Abstract

We study a 2-spin quantum Turing architecture, in which discrete local rotations $\{\alpha_m\}$ of the Turing head spin alternate with quantum controlled NOT-operations. We show that a single chaotic parameter input $\{\alpha_m\}$ leads to a chaotic dynamics in the entire Hilbert space. The instability of periodic orbits on the Turing head and 'chaos swapping' onto the Turing tape are demonstrated explicitly as well as exponential parameter sensitivity of the Bures metric.

1 Introduction

In recent years problems of quantum computing (QC) and information processing have received increasing attention. To solve certain classes of problems in a potentially very powerful way, one tries to utilize in QC the quantum-mechanical superposition principle and the (non-classical) entanglement [1], an undertaking which, at the same time, should contribute to our basic understanding of quantum mechanics itself (see e.g. [2]). However, building a large-scale quantum computer remains an extremely difficult task. The major obstacle is the coupling of the quantum computer to the environment, which tends to destroy quantum-mechanical superpositions very rapidly. This effect is usually referred to as decoherence. Present-day technology does not yet support the realization of a practical quantum computer. On the other hand, there might be interesting small-scale physics in a pure quantum regime based on a few pseudo-spins (qubits), which are realizable right now.

Chaotic behaviour as an exponential sensitivity to initial conditions has been well established in classical non-linear systems. The deterministic chaos, which occurs in non-dissipative systems, can typically be found starting from regular states as a function of some external control parameter. However, there seems to be no direct analogue to chaos in the quantum world: If two quantum states are initially almost identical (that is, their scalar product is very close to 1), they will remain so forever, since the Hamiltonian evolution is a unitary mapping which preserves scalar products. According to this negative result, the semiclassical 'quantum chaology' [3] has been constrained to studying some quantum-mechanical 'fingerprints of chaos' (like spectral properties), and non-trivial transitions from the quantum - to the classical domain and vice versa, following Bohr's correspondence principle (see e.g. [4, 5]). In addition, experimental progress in mesoscopic physics, e.g. the transport of electrons through so-called 'chaotic quantum dots' [6], has attracted a great deal of interest, the results of which give numerical evidence for weak chaos (indicated by level repulsion) [7, 8].

While most models of QC have been concerned with networks of quantum gates, which are reminiscent of classical integrated circuits, models based on quantum Turing machines (QTM) [9, 10] have been described along different lines but have not given rise

to much potential for future applications up to now. In both cases the complexity of the computation is characterized by sequences of unitary transformations (or the corresponding Hamiltonians $\hat{H}$ acting during finite time interval steps). The study of quantum chaos based on quantum gate networks has so far been proposed e.g. by implementing quantum baker's map on a 3-qubit NMR quantum computer [11], by realizing a quantum-mechanical delta-kicked harmonic oscillator or a harmonically driven oscillator in an ion trap [12, 13], and by showing quantum-mechanical localization of an ion in a trap [14, 15]. In all these cases some sort of sensitivity has been predicted with respect to parameters specifying the dynamics (e.g. the respective Hamiltonian).

Here we explicitly describe an iterative map with a few qubits which, though based on standard gates, can be thought to be realized as a QTM architecture: Local transformations of the Turing head controlled by a Fibonacci-like sequence of rotation angles alternate with a quantum-controlled NOT-operation with a second spin on the Turing tape. This chaotic control can generate a chaotic quantum propagation in the 'classical' regime [16], defined here as one with the Turing head being restricted to an entanglement-free state sequence ('primitive') [17]. It will then be shown that chaos on the Turing head can be found also for the quantum-mechanical superposition of those primitives, implying entanglement between head and tape as a genuine quantum feature ('non-classical regime'). Finally, due to this quantum correlation, we find a chaotic propagation even in the reduced subspace of the Turing tape ('chaos swapping'), and as a result also in the total network state $|\psi_n\rangle$. This behaviour should be contrasted with that of a regular QTM with its long-time revivals, which are absent in the 'chaotic' QTM.

2 Description of chaotically driven quantum Turing machine

The quantum network [18] to be considered is composed of N $(= M + 1)$ pseudo-spins $|p\rangle^{(\mu)}$; $p = 0, 1$; $\mu = S, 1, 2, \cdots, M$ (Turing-head S, Turing-tape spins $1, 2, \cdots, M$) so that its network state $|\psi\rangle$ lives in the 2^{M+1}-dimensional Hilbert space spanned by the product wavefunctions $|j^{(S)}k^{(1)}\cdots l^{(M)}\rangle = |jk\cdots l\rangle$. Correspondingly, any (unitary) network operator can be expanded as a sum of product operators. The latter may be based on the following $SU(2)$-generators

$$\begin{aligned} \hat{\lambda}_1^{(\mu)} &= \hat{P}_{01}^{(\mu)} + \hat{P}_{10}^{(\mu)}\,, \quad \hat{\lambda}_2^{(\mu)} = i\hat{P}_{01}^{(\mu)} - i\hat{P}_{10}^{(\mu)} \\ \hat{\lambda}_3^{(\mu)} &= \hat{P}_{11}^{(\mu)} - \hat{P}_{00}^{(\mu)}\,, \quad \hat{\lambda}_0^{(\mu)} = \hat{P}_{11}^{(\mu)} + \hat{P}_{00}^{(\mu)} = \hat{1}^{(\mu)}\,, \end{aligned} \tag{1}$$

where $\hat{P}_{pq}^{(\mu)} = |p\rangle^{(\mu)(\mu)}\langle q|$ is a (local) transition operator. For simplicity we restrict ourselves here to $M = 1$.

The initial state $|\psi_0\rangle$ will be taken to be a product of the Turing-head and tape wavefunctions. For the discretized dynamical description of the QTM we identify the unitary operators $\hat{U}_n$, $n = 1, 2, 3, \cdots$ (step number) with the local unitary transformation on the Turing-head S, $\hat{U}_{\alpha_m}^{(S)}$, and the quantum-controlled-NOT (QCNOT) on $(S, 1)$, $\hat{U}^{(S,1)}$, respectively, as follows:

$$\hat{U}_{2m-1} = \hat{U}_{\alpha_m}^{(S)} = \hat{1}^{(S)}\ \cos(\alpha_m/2) - \hat{\lambda}_1^{(S)}\ i\sin(\alpha_m/2) \tag{2}$$

$$\hat{U}_{2m} = \hat{U}^{(S,1)} = \hat{P}_{00}^{(S)}\,\hat{\lambda}_1^{(1)} + \hat{P}_{11}^{(S)}\,\hat{1}^{(1)} = \left(\hat{U}^{(S,1)}\right)^{\dagger} \quad , \tag{3}$$

where the Turing head is externally driven by the Fibonacci-like sequence $\alpha_{m+1} = \alpha_m + \alpha_{m-1}$ (mod 2π), $\alpha_0 = 0$. The mth Fibonacci number α_m is then controlled by α_1 via

$$\alpha_m \;=\; \frac{\alpha_1}{\sqrt{5}}\,(\beta^m - \gamma^m)\;, \tag{4}$$

where $\beta := \frac{1+\sqrt{5}}{2}$, $\gamma := \frac{1-\sqrt{5}}{2}$. The sequence $\{\alpha_m\}$ (mod 2π) acts as a chaotic input (Lyapunov exponent: $\ln\beta > 0$). It is useful for later calculations to note that

$$\begin{aligned} &\beta^{m+1} = \beta^m + \beta^{m-1}\,, \quad \gamma^{m+1} = \gamma^m + \gamma^{m-1} \\ &\beta^m = F(m)\cdot\beta + F(m-1)\,, \quad \gamma^m = F(m)\cdot\gamma + F(m-1)\,, \end{aligned} \tag{5}$$

where $F(m) := (\beta^m - \gamma^m)/\sqrt{5}$, the mth Fibonacci number with $F(1) = 1$. The chaotic sequence of Fibonacci-type can be interpreted as a temporal random (chaotic) analogue to 1-dimensional chaotic potentials in real space [19, 20].

First, we restrict ourselves to the reduced state-space dynamics of the head S and tape-spin 1, respectively,

$$\lambda_i^{(S)}(n) = \langle\psi_n|\hat{\lambda}_i^{(S)}\otimes\hat{1}^{(1)}|\psi_n\rangle\,,\;\; \lambda_k^{(1)}(n) = \langle\psi_n|\hat{1}^{(S)}\otimes\hat{\lambda}_k^{(1)}|\psi_n\rangle\,. \tag{6}$$

$|\psi_n\rangle$ is the total network state at step n, $\lambda_i^{(\mu)}(n)$ are the respective Bloch-vectors. We intend to show that these local propagations are chaotic, too. Due to the entanglement between the head and tape, both will, in general, appear to be in a 'mixed-state', which means that the length of the Bloch-vectors in (6) is less than 1. However, for specific initial states $|\psi_0\rangle$ the state of head and tape will remain pure: As $|\pm\rangle^{(1)} := \frac{1}{\sqrt{2}}\left(|0\rangle^{(1)} \pm |1\rangle^{(1)}\right)$ are the eigenstates of $\hat{\lambda}_1^{(1)}$ with $\hat{\lambda}_1^{(1)}|\pm\rangle^{(1)} = \pm|\pm\rangle^{(1)}$, the QCNOT-operation $\hat{U}^{(S,1)}$ of equation (3) cannot create any entanglement, irrespective of the head state $|\varphi\rangle^{(S)}$, i.e.

$$\begin{aligned} \hat{U}^{(S,1)}\,|\varphi\rangle^{(S)}\otimes|+\rangle^{(1)} &= |\varphi\rangle^{(S)}\otimes|+\rangle^{(1)} \\ \hat{U}^{(S,1)}\,|\varphi\rangle^{(S)}\otimes|-\rangle^{(1)} &= \hat{\lambda}_3^{(S)}|\varphi\rangle^{(S)}\otimes|-\rangle^{(1)}\,. \end{aligned} \tag{7}$$

As a consequence, the state $|\psi_n\rangle$ remains a product state at any step n for the initial product states $|\psi_0^{\pm}\rangle = |\varphi_0\rangle^{(S)}\otimes|\pm\rangle^{(1)}$ with $|\varphi_0\rangle^{(S)} = \cos(\varphi_0/2)|0\rangle^{(S)} - i\sin(\varphi_0/2)|1\rangle^{(S)}$ and the Turing head then performs a pure-state trajectory ('primitive') on the Bloch-circle $\left(\lambda_1^{(S)}(n) = 0\right)$

$$|\psi_n^{\pm}\rangle = |\varphi_n^{\pm}\rangle^{(S)}\otimes|\pm\rangle^{(1)}\,, \quad \left(\lambda_2^{(S)}(n|\pm)\right)^2 + \left(\lambda_3^{(S)}(n|\pm)\right)^2 = 1\,. \tag{8}$$

Here $\lambda_j^{(S)}(n|\pm)$ denotes the Bloch-vector of the Turing head S conditioned by the initial state $|\psi_0^{\pm}\rangle$. From the Fibonacci relation and the property (7) it is found for $|\varphi_n^{+}\rangle^{(S)}\otimes|+\rangle^{(1)}, n = 2m$, and $\varphi_0^{\pm} = \alpha_0 = 0$ that

$$\lambda_2^{(S)}(2m|+) = \sin\mathcal{C}_{2m}(+)\,, \quad \lambda_3^{(S)}(2m|+) = -\cos\mathcal{C}_{2m}(+)\,, \tag{9}$$

where $\mathcal{C}_{2m}(+) := \sum_{j=1}^{m} \alpha_j$, and $\lambda_k^{(S)}(2m-1|+) = \lambda_k^{(S)}(2m|+)$. In order to derive the corresponding expression of $\lambda_k^{(S)}(n|-)$ for $|\varphi_n^-\rangle^{(S)} \otimes |-\rangle^{(1)}$, we utilize the following recursion relations for the cumulative rotation angle $\mathcal{C}_n(-)$ up to step n

$$\mathcal{C}_{2m}(-) = -\mathcal{C}_{2m-1}(-)\,, \quad \mathcal{C}_{2m-1}(-) = \alpha_m + \mathcal{C}_{2m-2}(-)\,. \tag{10}$$

Then $\mathcal{C}_{2m}(-), \mathcal{C}_{2m-1}(-)$, respectively, satisfy the following expressions:

$$\begin{aligned} \mathcal{C}_{2m}(-) &= -\mathcal{C}_{2m-2}(-) - \alpha_m = (-1)^{m-1} \sum_{j=1}^{m} (-1)^j \alpha_j \\ \mathcal{C}_{2m-1}(-) &= -\mathcal{C}_{2m-3}(-) + \alpha_m = (-1)^{m} \sum_{j=1}^{m} (-1)^j \alpha_j\,, \end{aligned} \tag{11}$$

yielding $\lambda_2^{(S)}(n|-) = \sin \mathcal{C}_n(-)$, $\lambda_3^{(S)}(n|-) = -\cos \mathcal{C}_n(-)$ [*cf.* (9)]. The Fibonacci property implies that both primitives, $|\varphi_n^+\rangle^{(S)} \otimes |+\rangle^{(1)}$ and $|\varphi_n^-\rangle^{(S)} \otimes |-\rangle^{(1)}$, are chaotically driven.

From any initial state, $|\psi_0\rangle = a^{(+)}|\varphi_0^+\rangle^{(S)} \otimes |+\rangle^{(1)} + a^{(-)}|\varphi_0^-\rangle^{(S)} \otimes |-\rangle^{(1)}$, we then obtain at step n

$$|\psi_n\rangle = a^{(+)}|\varphi_n^+\rangle^{(S)} \otimes |+\rangle^{(1)} + a^{(-)}|\varphi_n^-\rangle^{(S)} \otimes |-\rangle^{(1)} \tag{12}$$

and, observing the orthogonality of the $|\pm\rangle^{(1)}$,

$$\lambda_k^{(S)}(n) = |a^{(+)}|^2\, \lambda_k^{(S)}(n|+) + |a^{(-)}|^2\, \lambda_k^{(S)}(n|-)\,. \tag{13}$$

This trajectory of the Turing-head S represents a non-orthogonal pure-state decomposition. By using (9), (11), (13) $\left(\text{with } a^{(+)} = a^{(-)} = 1/\sqrt{2}\right)$ we finally have for $|\psi_0\rangle = |0\rangle^{(S)} \otimes |0\rangle^{(1)}$

$$\begin{aligned} \left(\lambda_2^{(S)}(2m),\, \lambda_3^{(S)}(2m)\right) &= \cos \mathcal{A}_m \cdot (\sin \mathcal{B}_m,\, -\cos \mathcal{B}_m) \\ \left(\lambda_2^{(S)}(2m-1),\, \lambda_3^{(S)}(2m-1)\right) &= \cos \mathcal{B}_m \cdot (\sin \mathcal{A}_m,\, -\cos \mathcal{A}_m)\,, \end{aligned} \tag{14}$$

where $\mathcal{A}_m := \alpha_m + \alpha_{m-2} + \cdots$, $\mathcal{B}_m := \alpha_{m-1} + \alpha_{m-3} + \cdots$. The expression (14) indicates that also in the 'non-classical' regime the local dynamics of the Turing head is controlled by a 'chaotic' driving force, since the sequences $\mathcal{A}_m$ and $\mathcal{B}_m$, namely $\{\alpha_{2m}\}$ (mod 2π) or $\{\alpha_{2m-1}\}$ (mod 2π), respectively, are in fact both chaotic, as $\{\alpha_m\}$ (mod 2π) is.

The Bloch-vector $\vec{\lambda}^{(S)}(n)$ can alternatively be calculated directly from the initial state $\left(\text{here: } |\psi_0\rangle = |0\rangle^{(S)} \otimes |0\rangle^{(1)}\right)$ and for any control angle α_1 by using equation (14) and the relations

$$\begin{aligned} \mathcal{A}_m &= \begin{cases} \frac{\alpha_1}{\sqrt{5}}\,(\beta^{m+1} - \gamma^{m+1}) & m = \text{odd} \\ \frac{\alpha_1}{\sqrt{5}}\left(\beta^{m+1} - \gamma^{m+1} - \sqrt{5}\right) & m = \text{even} \end{cases} \\ \mathcal{B}_m &= \begin{cases} \frac{\alpha_1}{\sqrt{5}}\left(\beta^{m} - \gamma^{m} - \sqrt{5}\right) & m = \text{odd} \\ \frac{\alpha_1}{\sqrt{5}}\,(\beta^{m} - \gamma^{m}) & m = \text{even}\,, \end{cases} \end{aligned} \tag{15}$$

demonstrating a striking computational reducibility in that one needs for calculating $\vec{\lambda}^{(S)}(n)$ neither the total network state $|\psi_n\rangle$ nor to follow up each individual step n.

3 Instability of periodic orbits

Now we verify that the periodic orbits on the plane $\left\{0, \lambda_2^{(S)}, \lambda_3^{(S)}\right\}$ are unstable, which proves that the dynamics of the Turing head ('output') is indeed chaotic (figure 1). Because of the alternating character of the dynamics, equations (2), (3), it suffices to check the periodicity only for step $n = 2m$: The periodic orbits for $\lambda_2^{(S)}(0) = 0, \lambda_3^{(S)}(0) = -1$ must obey two constraints, $\mathcal{C}_{2m}(+) = \mathcal{C}_{2m}(-) \stackrel{!}{=} 2\pi p$, $p \in \mathbf{Z}$ and $\alpha_{m+1} = \alpha_1 \pmod{2\pi}$ for $n = 2m+1$ (one concludes that α_1 must be a rational multiple of π). By using the Fibonacci numbers (4), one finds $\mathcal{C}_{2m}^{\rm per}(+)$ in (9) and $\mathcal{C}_{2m}^{\rm per}(-)$ in (11), respectively, for period $= 2m$ as

$$\begin{aligned} \mathcal{C}_{2m}^{\rm per}(+) &= \frac{\alpha_1}{\sqrt{5}}\left(\beta^{m+2} - \gamma^{m+2} - \sqrt{5}\right) \\ \mathcal{C}_{2m}^{\rm per}(-) &= \frac{\alpha_1}{\sqrt{5}}\left(-\beta^{m-1} + \gamma^{m-1} + (-1)^m\sqrt{5}\right) . \end{aligned} \tag{16}$$

Then let us consider a small perturbation δ of the initial phase angle $\alpha_0 = 0$, implying $|\varphi_0\rangle^{(S)} = \cos(\delta/2)|0\rangle - i\sin(\delta/2)|1\rangle$ and a perturbed Fibonacci-like sequence $\{\alpha'_m\}$ (mod 2π):

$$\alpha'_0 = \delta,\ \alpha'_1 = \alpha_1,\ \alpha'_2 = \alpha_1 + \delta, \cdots . \tag{17}$$

Similarly to (16), we obtain for this case $\mathcal{C}'_{2m}(\pm) = \mathcal{C}_{2m}^{\rm per}(\pm) + \Delta\mathcal{C}_{2m}(\pm)$, where the deviation terms from the periodic orbits read, respectively,

$$\begin{aligned} \Delta\mathcal{C}_{2m}(+) &= \frac{\delta}{\sqrt{5}}\left(\beta^{m+1} - \gamma^{m+1}\right) \\ \Delta\mathcal{C}_{2m}(-) &= -\frac{\delta}{\sqrt{5}}\left(\beta^{m-2} - \gamma^{m-2}\right) . \end{aligned} \tag{18}$$

By using (18), we are able to represent the evolution of the perturbation, $\Delta\lambda_j^{(S)}(n)$, at the $n = 2m$-th step for the Turing-head dynamics as

$$\begin{pmatrix} \Delta\lambda_2^{(S)}(2m) \\ \Delta\lambda_3^{(S)}(2m) \end{pmatrix} = \begin{pmatrix} M_{11} & 0 \\ 0 & M_{22} \end{pmatrix} \begin{pmatrix} \Delta\lambda_2^{(S)}(0) \\ \Delta\lambda_3^{(S)}(0) \end{pmatrix} , \tag{19}$$

where $\Delta\lambda_2^{(S)}(0) = \sin\delta$, $\Delta\lambda_3^{(S)}(0) = -\cos\delta$; $\Delta\lambda_2^{(S)}(2m) = \cos(\delta\alpha_m)\sin(\delta\alpha_{m-1})$, $\Delta\lambda_3^{(S)}(2m) = -\cos(\delta\alpha_m)\cos(\delta\alpha_{m-1})$; $M_{11} = \cos(\delta\alpha_m)\sin(\delta\alpha_{m-1})\ /\sin\delta$, $M_{22} = \cos(\delta\alpha_m)\cos(\delta\alpha_{m-1})/\cos\delta$, respectively. One easily shows [*cf.* equation (5)] that

$$\lim_{\delta\to 0} M_{11} = F(m-1) = \frac{1}{\sqrt{5}}\left(\beta^{m-1} - \gamma^{m-1}\right) \qquad \lim_{\delta\to 0} M_{22} = 1 , \tag{20}$$

which means that M_{11} grows exponentially (note that $\beta > 1, |\gamma| < 1$), and the periodic orbit on the Turing head is thus unstable to any small perturbation δ in the external control.

As an explicit example consider the case of $\alpha_1 = \frac{2\pi}{5}$ with $|\psi_0\rangle = |0\rangle^{(S)} \otimes |0\rangle^{(1)}$: By using equation (5) in equation (16) for $\mathcal{C}_{2m}^{\rm per}(+) = 2\pi p$ the periodic orbits with period $= 2m$ have to obey $F(m+2) = 1 \pmod 5$. Together with the second condition, $F(m+1) = 1 \pmod 5$ for $n = 2m+1$, we obtain $F(m-1) = 1$, $F(m) = 0 \pmod 5$. For $\mathcal{C}_{2m}^{\rm per}(-) = 2\pi p$ it

follows likewise that $F(m-1) = 1 \pmod 5$ for $m =$ even, $F(m-1) = 4 \pmod 5$ for $m =$ odd. Considering the common condition for both cases, $F(m-1) = 1$ and $F(m) = 0 \pmod 5$, we find the smallest m satisfying both conditions, namely $m = 20$, i.e. $n = 2m = 40$. $\left[\lim_{\delta\to 0} M_{11} = F(19) = 4181 \gg 1, \text{see figure 2}\right]$.

Remarkably enough, the local dynamics of the Turing tape also contains some exponential sensitivity to initial conditions $\left[\text{here: } |\psi_0\rangle = |0\rangle^{(S)} \otimes |0\rangle^{(1)}, \lambda_1^{(1)}(n) = \lambda_2^{(1)}(n) = 0\right]$:

$$\lambda_3^{(1)}(n) = \begin{cases} -\cos\left(\alpha_{\left[\frac{n}{2}\right]+1} - \alpha_1 + \delta^{\mathrm{Fib}}_{\left[\frac{n}{2}\right]}\right) & n = 0, 1 \pmod 4 \\ \cos\left(\alpha_{\left[\frac{n}{2}\right]+1} + \delta^{\mathrm{Fib}}_{\left[\frac{n}{2}\right]}\right) & n = 2, 3 \pmod 4\,, \end{cases} \tag{21}$$

where $\delta_m^{\mathrm{Fib}} := \frac{\delta}{\sqrt{5}}(\beta^m - \gamma^m)$; $[a] := n$, $a = n + r$, $n \in \mathbf{Z}$, $0 \le r < 1$. One easily confirms that there is no periodic orbit with period $2m = 2 \pmod 4$. The following expression for the deviation from the periodic orbits with period $2m = 0 \pmod 4$ at step $n = 2m + 2$ holds:

$$\Delta\lambda_3^{(1)}(2m+2) = M \cdot \Delta\lambda_3^{(1)}(2)\,, \quad \lim_{\delta\to 0} M = \frac{1}{\sqrt{5}}\left(\beta^{m+1} - \gamma^{m+1}\right)\frac{\sin(\alpha_{m+2})}{\sin(\alpha_1)}\,, \tag{22}$$

with $\Delta\lambda_3^{(1)}(2) = \cos(\alpha_1 + \delta) - \cos(\alpha_1)$, $\Delta\lambda_3^{(1)}(2m+2) = \cos(\alpha_{m+2} + \delta_{m+1}) - \cos(\alpha_{m+2})$; the perturbation δ in (17) does not enter into the Turing-tape dynamics until $n = 2$! Equation (22) shows the exponential instability of the periodic orbit. Indeed, the Turing tape exhibits chaos only by means of the entanglement with the head ('chaos swapping'), not as a result of a direct chaotic driving force.

4 Exponential parameter sensitivity

The distance between density operators, $\hat\rho$ and $\hat\rho'$, defined by the so-called Bures metric [21]

$$D^2_{\rho\rho'} := \mathrm{Tr}\left\{(\hat\rho - \hat\rho')^2\right\}\,. \tag{23}$$

lies, independent of the dimension of the Liouville space, between 0 and 2 [the maximum (squared) distance of 2 applies to pure orthogonal states, $D^2 = 2\,(1 - |\langle\psi|\psi'\rangle|^2)$]. This metric can be applied to the total-network-state space or any subspace. In any case it is a convenient additional means to characterize various QTMs: For $\alpha_m = \alpha_1$ (Lyapunov exponent = 0) [17] and any δ the distance remains almost constant (see figure 3*d*); for the Fibonacci-like driving force, on the other hand, $\left(\alpha_m(\hat\rho) = \alpha_m, \alpha_m(\hat\rho') = \alpha_m(\hat\rho) + \delta^{\mathrm{Fib}}_{m-1}\right)$ we obtain an initial exponential sensitivity, which is eventually constrained, though, by $D^2 \le 2$ (see figure 3*a* - *c*). It is instructive to consider another regular QTM controlled by the rule $\alpha_{m+1} = 2\alpha_m - \alpha_{m-1}$ (Lyapunov exponent = 0): $\alpha_m(\hat\rho) = m\alpha_1, \alpha_m(\hat\rho') = \alpha_m(\hat\rho) - (m-1)\,\delta$. Here we observe a revival in the evolution of D^2, which confirms that periodic orbits are stable (figure 3*d*), whereas there is no revival for the above chaotic system. Finally we

display the evolution of D^2 for the total network state $|\psi_n\rangle$, which also shows exponential sensitivity. The respective distances for tape-spin 1 are similar to those shown.

The ultimate source of the present chaotic behaviour is that any small perturbation δ to the initial state, $|\psi_0(\delta)\rangle$, is connected with a perturbed unitary evolution, $\hat{U}(\delta)$, which implies that the scalar product between different initial states (as a measure of distance) is no longer conserved under these evolutions:

$$O' := |\langle\psi_0(\delta)|\hat{U}^\dagger(\delta)\,\hat{U}(0)|\psi_0(0)\rangle|^2\,, \quad D^2 = 2(1-O')\,. \tag{24}$$

Thus the initial state is directly correlated to its unitary evolution, which can lead to the exponential sensitivity to initial condition, whereas there is no chaos in a generic quantum system evolving by a fixed $\hat{U}$ even if characterized by chaotic input parameters. This O' reminds us immediately of the test function $O = |\langle\psi|\hat{V}^\dagger(t)\,\hat{U}(t)|\psi\rangle|^2$ [22], where $\hat{U}, \hat{V}$ are specified by slightly different external parameters: The corresponding parameter-sensitivity has been proposed as a measure to distinguish quantum chaos from regular quantum dynamics. The origin of chaos in our QTM may thus be alternatively ascribed to a perturbed $\hat{V} = \hat{U}(\delta)$ in the control (*cf.* the comment by R. Schack [23]).

5 Summary

In conclusion, we have studied the quantum dynamics of a small chaotically driven QTM based on a decoherence-free Hamiltonian. Quantum chaos has been shown to occur as an exponential parameter-sensitivity and a cumulative loss of control in a pure quantum regime. This might be contrasted with the usual quantum chaology, which is concerned essentially with semiclassical spectrum analysis of classically chaotic systems (e.g. level spacing, spectral rigidity). As quantum features we utilized the superposition principle and the physics of entanglement. Our dynamical chaos manifests itself in the superposition and entanglement of a pair of 'classical' (i.e. unentangled) chaotic state-sequences. Due to the entanglement, we can see the chaos in any local Bloch-plane. This indicates that patterns in reduced Bloch-spheres (a quantum version of a Poincaré-cut, figure 2) should be useful to characterize quantum chaos in a broad class of quantum networks: Here, a periodic orbit would be represented by finite set of fixed points on the plane $\left\{0, \lambda_2^{(S)}, \lambda_3^{(S)}\right\}$. It is noteworthy that this kind of control loss is completely different from the typical control limit of a quantum network resulting from the exponential blow-up of Hilbert-space dimension in which the state evolves [24]. It is expected that a QTM architecture with a larger number of pseudo-spins on the Turing tape would also exhibit chaos under the same type of driving. However, it is just the chaos in small networks which might be interesting for experimental studies, especially in the form of ensembles thereof. The Fibonacci-like sequence should, however, be considered but a special example for chaotic input. Such inputs would, of course, have to be avoided in quantum computation; otherwise the resulting quantum dynamics would easily become chaotic in its entirety!

6 Acknowledgements

We thank C. Granzow, M. Karremann, A. Otte and, P. Pangritz for fruitful discussions, and especially P. Pangritz for numerical results. One of us (I. K.) acknowledges D. Braun and S. Gnutzmann for useful references.

References

[1] E. Schrödinger, 1935, *Naturwissenschaften*, **23**, 807, 823 and 844, reprinted in English in: J. A. Wheeler and W. H. Zurek, 1983, *Quantum Theory of Measurement* (Princeton U. P., Princeton, N. J.).

[2] S. Dürr, T. Nonn, and G. Rempe, 1998, *Nature*, **395**, 33.

[3] M. V. Berry, 1985, *Proc. R. Soc. London A*, **400**, 229; 1987, *Proc. R. Soc. London A*, **413**, 183; 1989, *Physica Scripta* **40**, 335.

[4] J. Ford, G. Mantica, and G. H. Ristow, 1991, *Physica D*, **50**, 493.

[5] F. Haake, 1991, *Quantum Signatures of Chaos* (Springer, New York).

[6] L. P. Kouwenhoven *et al.*, 1997, in *Mesoscopic Electron Transport*, edited by L. L. Sohn *et al.*, NATO ASI Series E345 (Kluwer, Dordrecht).

[7] D. L. Shepelyansky, 1994, *Phys. Rev. Lett.*, **73**, 2607.

[8] X. Waintal and J-L. Pichard, 1998, *Eur. Phys. J. B*, **6**, 117; X. Waintal, D. Weinmann, and J-L. Pichard, 1999, *Eur. Phys. J. B*, **7**, 451.

[9] P. Benioff, 1982, *Phys. Rev. Lett.*, **48**, 1581; 1996, *Phys. Rev. A*, **54**, 1106; 1998, *Fortschr. Physik*, **46**, 423.

[10] D. Deutsch, 1985, *Proc. R. Soc. London A*, **400**, 97; 1989, *Proc. R. Soc. London A*, **425**, 73.

[11] R. Schack, 1998, *Phys. Rev. A*, **57**, 1634; T. Brun and R. Schack, quant-ph/9807050.

[12] S. A. Gardiner, J. I. Cirac, and P. Zoller, 1997, *Phys. Rev. Lett.*, **79**, 4790; Erratum, 1998, *Phys. Rev. Lett.*, **80**, 2968.

[13] G. P. Bergman *et al.*, quant-ph/9903063.

[14] M. E. Ghafar *et al.*, 1997, *J. Mod. Optics*, **44**, 1985; 1997, *Phys. Rev. Lett.*, **78**, 4181.

[15] K. Riedel *et al.*, 1999, *Phys. Rev. A*, **59**, 797.

[16] R. Blümel, 1994, *Phys. Rev. Lett.*, **73**, 428.

[17] I. Kim and G. Mahler, 1999, *Phys. Rev. A*, **60**, 692.

[18] G. Mahler and V. A. Weberruß, 1998, *Quantum Networks: Dynamics of Open Nanostructures* (2nd ed. Springer, New York).

[19] M. Kohmoto, L. P. Kadanoff, and C. Tang, 1983, *Phys. Rev. Lett.*, **50**, 1870.

[20] F. Piéchon, M. Benakli, and A. Jagannathan, 1995, *Phys. Rev. Lett.*, **74**, 5248.

[21] M. Hübner, 1992, *Phys. Lett. A*, **163**, 293; 1993, *Phys. Lett. A*, **179**, 226.

[22] A. Peres, 1991, in *Quantum Chaos*, edited by H. A. Cerdeira *et al.* (World Scientific, Singapore); 1993, *Quantum Theory: Concepts and Methods* (Kluwer, Dordrecht).

[23] R. Schack, 1995, *Phys. Rev. Lett.*, **75**, 581.

[24] R. P. Feynman, 1982, *Int. J. theor. Phys.*, **21**, 467.

Figure 1: A input-output scheme of our quantum Turing machine (QTM).

Figure 2: Turing-head patterns $\{0, \lambda_2(n), \lambda_3(n)\}$ under Fibonacci control for initial state $|\psi_0\rangle = |0\rangle^{(S)} \otimes |0\rangle^{(1)}$. (a): $\alpha_1 = \frac{2}{5}\pi$ (periodic); (b): $\alpha_1 = \frac{2}{5} \times 3.141592654$ (aperiodic) and total step number $n = 10000$.

Figure 3: Evolution of the (squared) distance $D^2_{\rho\rho'}$ between QTM state with $(\hat{\rho}')$ and without $(\hat{\rho})$ perturbation δ. $\alpha_1 = \frac{2}{5}\pi$, $|\psi_0\rangle = |0\rangle^{(S)} \otimes |0\rangle^{(1)}$ for $\hat{\rho}$, and $\Big(\cos(\delta/2)|0\rangle^{(S)} - i\sin(\delta/2)|1\rangle^{(S)}\Big) \otimes |0\rangle^{(1)}$ for $\hat{\rho}'$. (a): chaotic input according to equation (4) (inset shows initial behaviour in more detail; *cf.* Table 1) for the Turing-head state, $\delta = 0.001$; (b): the same as (a) but for $\delta = 0.00001$; (c): the same as (a) for total network state $|\psi_n\rangle$; (d): $D^2_{\rho\rho'}$ within the Turing head subspace for $\alpha_m = \alpha_1$ ($D^2 \approx 0$, solid line A, $\delta = 0.001, 0.0005$) and $\alpha_{m+1} = 2\alpha_m - \alpha_{m-1}$ (dotted line B, $\delta = 0.001$; boxed line C, $\delta = 0.0005$), inset shows line B on larger scale.

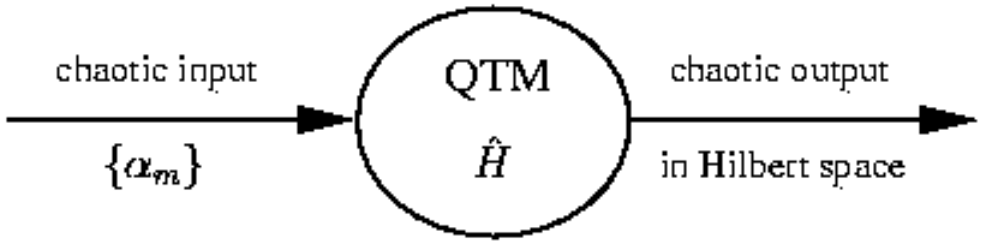
chaotic input
$\{\alpha_m\}$
QTM
$\hat{H}$
chaotic output
in Hilbert space

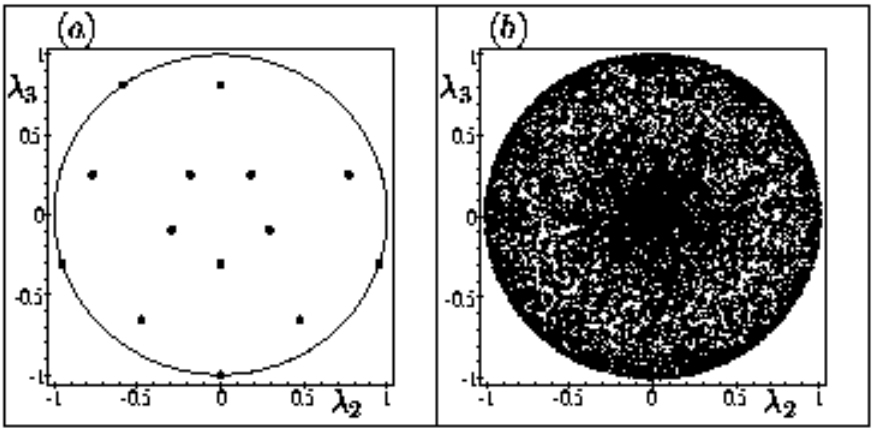
(a)
(b)
λ_3
λ_2

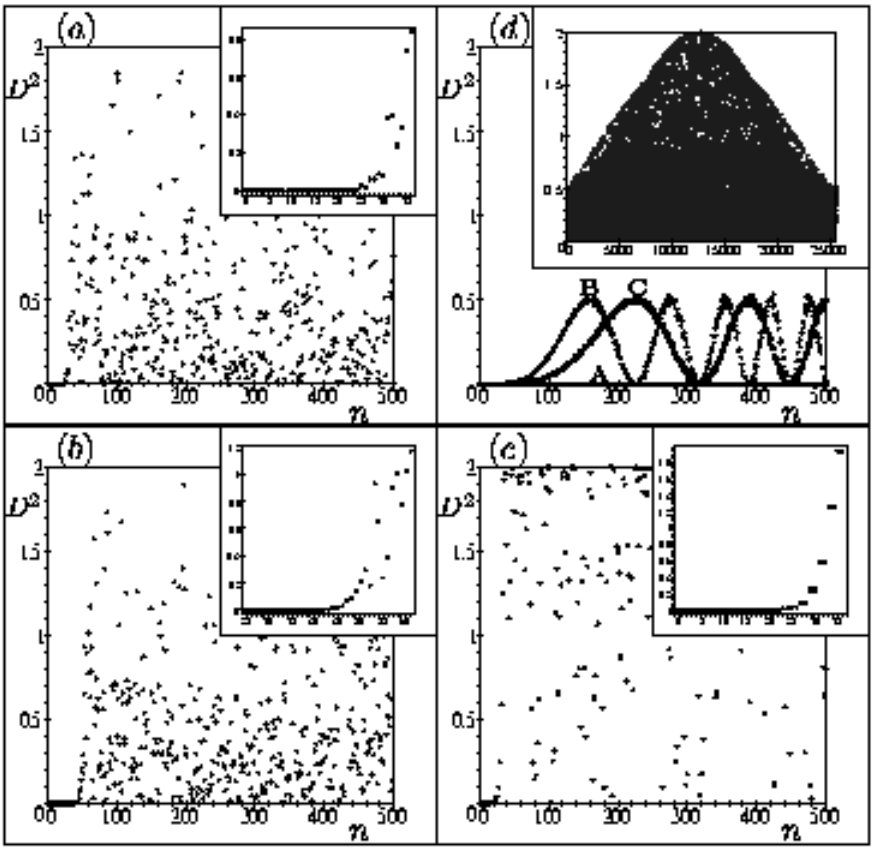
(a)
(d)
(b)
(c)
B
C
n

Table 1: Analytical evolution of (squared) distance $D^2_{\rho\rho'}$ between the Turing-head states as of Fig 3*a*: With increasing time step n the originally small phase angle grows at a Fibonacci-like rate (separately for $n =$ even and $n =$ odd), such that D^2 shows exponential growth initially and then wild oscillations between 0 and 2.

n	$D^2_{\rho\rho'}(n)$
0	$1-\cos(\mathbf{1}\delta)$
1	$1-\cos(\mathbf{1}\delta)$
2	$\frac{1}{2}+\frac{1}{4}\cos(2\alpha_1+\mathbf{2}\delta)-\frac{1}{2}\cos(2\alpha_1+\mathbf{1}\delta)-\frac{1}{2}\cos(\mathbf{1}\delta)+\frac{1}{4}\cos(2\alpha_1)$
3	$\frac{1}{4}-\frac{1}{4}\cos(\mathbf{2}\delta)$
4	$\frac{1}{4}-\frac{1}{4}\cos(\mathbf{2}\delta)$
5	$\frac{1}{2}-\frac{1}{4}\cos(2\alpha_1+\mathbf{3}\delta)-\frac{1}{4}\cos(\mathbf{3}\delta)+\frac{1}{4}\cos(2\alpha_1+\mathbf{2}\delta)$ $-\frac{1}{4}\cos(2\alpha_1-\mathbf{1}\delta)-\frac{1}{4}\cos(\mathbf{1}\delta)+\frac{1}{4}\cos(2\alpha_1)$
6	$\frac{1}{2}+\frac{1}{4}\cos(6\alpha_1+\mathbf{4}\delta)-\frac{1}{4}\cos(6\alpha_1+\mathbf{3}\delta)-\frac{1}{4}\cos(\mathbf{3}\delta)$ $-\frac{1}{4}\cos(6\alpha_1+\mathbf{1}\delta)-\frac{1}{4}\cos(\mathbf{1}\delta)+\frac{1}{4}\cos(6\alpha_1)$
7	$\frac{1}{2}-\frac{1}{4}\cos(6\alpha_1+\mathbf{5}\delta)-\frac{1}{4}\cos(\mathbf{5}\delta)+\frac{1}{4}\cos(6\alpha_1+\mathbf{4}\delta)$ $-\frac{1}{4}\cos(6\alpha_1-\mathbf{1}\delta)-\frac{1}{4}\cos(\mathbf{1}\delta)+\frac{1}{4}\cos(6\alpha_1)$
8	$\frac{1}{2}+\frac{1}{4}\cos(8\alpha_1+\mathbf{6}\delta)-\frac{1}{4}\cos(8\alpha_1+\mathbf{5}\delta)-\frac{1}{4}\cos(\mathbf{5}\delta)$ $-\frac{1}{4}\cos(8\alpha_1+\mathbf{1}\delta)-\frac{1}{4}\cos(\mathbf{1}\delta)+\frac{1}{4}\cos(8\alpha_1)$
9	$\frac{1}{2}-\frac{1}{4}\cos(8\alpha_1+\mathbf{8}\delta)-\frac{1}{4}\cos(\mathbf{8}\delta)+\frac{1}{4}\cos(8\alpha_1+\mathbf{6}\delta)$ $-\frac{1}{4}\cos(8\alpha_1-\mathbf{2}\delta)-\frac{1}{4}\cos(\mathbf{2}\delta)+\frac{1}{4}\cos(8\alpha_1)$
10	$\frac{1}{2}+\frac{1}{4}\cos(16\alpha_1+\mathbf{10}\delta)-\frac{1}{4}\cos(16\alpha_1+\mathbf{8}\delta)-\frac{1}{4}\cos(\mathbf{8}\delta)$ $-\frac{1}{4}\cos(16\alpha_1+\mathbf{2}\delta)-\frac{1}{4}\cos(\mathbf{2}\delta)+\frac{1}{4}\cos(16\alpha_1)$
11	$\frac{1}{2}-\frac{1}{4}\cos(16\alpha_1+\mathbf{13}\delta)-\frac{1}{4}\cos(\mathbf{13}\delta)+\frac{1}{4}\cos(16\alpha_1+\mathbf{10}\delta)$ $-\frac{1}{4}\cos(16\alpha_1-\mathbf{3}\delta)-\frac{1}{4}\cos(\mathbf{3}\delta)+\frac{1}{4}\cos(16\alpha_1)$
12	$\frac{1}{2}+\frac{1}{4}\cos(24\alpha_1+\mathbf{16}\delta)-\frac{1}{4}\cos(24\alpha_1+\mathbf{13}\delta)-\frac{1}{4}\cos(\mathbf{13}\delta)$ $-\frac{1}{4}\cos(24\alpha_1+\mathbf{3}\delta)-\frac{1}{4}\cos(\mathbf{3}\delta)+\frac{1}{4}\cos(24\alpha_1)$